

Lattice parameters and local atomic structure of silicon-rich Si-Ge/Si (100) films

M. Matsuura,* J. M. Tonnerre,[†] and G. S. Cargill III

IBM Research Division, Thomas J. Watson Research Center, Yorktown Heights, New York 10598

(Received 4 April 1991)

The lattice parameters and Ge-to-Si nearest-neighbor and next-nearest-neighbor distances were measured using x-ray rocking curves and extended x-ray-absorption fine-structure spectroscopy for four different Si-rich $\text{Si}_{1-x}\text{Ge}_x/\text{Si}(100)$ epitaxial films. The Si-Ge films, two prepared by molecular-beam epitaxy and two by chemical-vapor deposition, had thicknesses of 500-900 Å and Ge concentrations of $x_{\text{Ge}}=0.06-0.18$. Lattice parameters of the films, corrected for coherency strain, agreed with values reported for bulk Si-Ge alloys. Ge-to-Si distances were 2.375 ± 0.02 Å and 3.85 ± 0.06 Å for nearest and next-nearest neighbors, respectively, and were independent of Ge concentration within these experimental uncertainties. A simple, random-solid-solution model using composition-independent values for nearest-neighbor distances $r_{\text{Si-Si}}$, $r_{\text{Ge-Ge}}$, and $r_{\text{Ge-Si}}$ reproduced the average nearest-neighbor distance $\langle r \rangle(x_{\text{Ge}})$ deduced from observed lattice parameters $a(x_{\text{Ge}})$ for our range of Ge concentrations. Composition variations of interatomic distances expected from various theoretical models [Martins and Zunger, *Phys. Rev. B* **30**, 6217 (1984); Shih *et al.*, *B* **31**, 1139 (1985); Thorpe and Garboczi, *Bull. Am. Phys. Soc.* **35**, 781 (1990)] all fell within our experimental uncertainty of ± 0.02 Å.

I. INTRODUCTION

The lattice mismatch between an epitaxial film and a substrate induces lattice strain and may create misfit dislocations in the film. Therefore understanding and control of the lattice mismatch are important for achieving defect-free epitaxial films. In some cases Vegard's law¹ is a simple and useful guide for estimating lattice parameter change due to impurity doping or alloying. But as reported earlier,^{2,3} the lattice parameter of heavily doped Si:As shows lattice contraction rather than expansion, in spite of As having a larger atomic size than Si, based on extended x-ray absorption fine-structure (EXAFS) measurements.⁴ In this case conduction electrons due to As doping contribute negatively to the lattice parameters, and this effect is not included in the simple application of Vegard's law, which would predict, incorrectly, a lattice parameter increase from adding As to Si.

For cases of heterovalent impurities, like As in Si or Ga in Si, to determine experimentally the quantitative effect of added electrons or holes on the lattice parameter, it is necessary to evaluate separately the effect of atom size differences on the lattice parameter, which has been done using EXAFS measurements and Vegard's law.^{2,3,5} Although reasonable results have been obtained for Si:As and Si:Ga in this way, it would be desirable to test how accurately this procedure works, for example, in the case of isovalent impurities, which involve no doping effects. This is one of our motivations for the present investigation of Si-Ge alloys.⁶ Another motivation is to determine the dependence of Ge-Si nearest-neighbor distances on alloy composition for comparison with theoretical predictions.⁷⁻⁹

There have been previous investigations of lattice parameter change with the concentration for Si-Ge bulk al-

loys,¹⁰ but studies of lattice parameters for Si-Ge epitaxial films are very limited.^{11,12} Bulk Si-Ge alloys have shown a slight negative deviation from Vegard's law, and several theoretical explanations have been offered for this negative deviation.¹⁰ Previous EXAFS studies of Ge in Si-Ge alloys were limited to a single composition ($x=0.31$) crystalline alloy¹² or were limited to amorphous Si-Ge alloy films.¹³

In the present work we have measured EXAFS as well as x-ray rocking curves (XRC's) for silicon-rich $\text{Si}_{1-x}\text{Ge}_x$ ($0.06 \leq x_{\text{Ge}} \leq 0.18$) epitaxial films made by molecular-beam epitaxy (MBE) and by chemical-vapor deposition (CVD) on (100) Si substrates.

In order to understand the concentration dependence of the lattice parameters, which reflect average interatomic distances, it is necessary to consider the relationship between lattice parameters, as determined from x-ray rocking curves, and interatomic distances, as determined from EXAFS measurements. A simple random-solid-solution model has been used to explain the observed composition dependence of lattice parameters for the Si-rich Si-Ge alloy films in terms of the nearest-neighbor distances. Section II of this paper describes the samples and experiments performed on them. Experimental results are discussed in Sec. III, followed by a summary of conclusions in Sec. IV.

II. SAMPLES AND EXPERIMENTS

A. Epitaxial films and RBS

Four silicon-rich $\text{Si}_{1-x}\text{Ge}_x$ epitaxial films were grown on Si(100) substrates. Two of them, MBE1 and MBE2, were made by molecular-beam epitaxy¹⁴ and two others, CVD1 and CVD2, by chemical-vapor deposition.¹⁵ The Ge concentrations of the films were determined by Ruth-

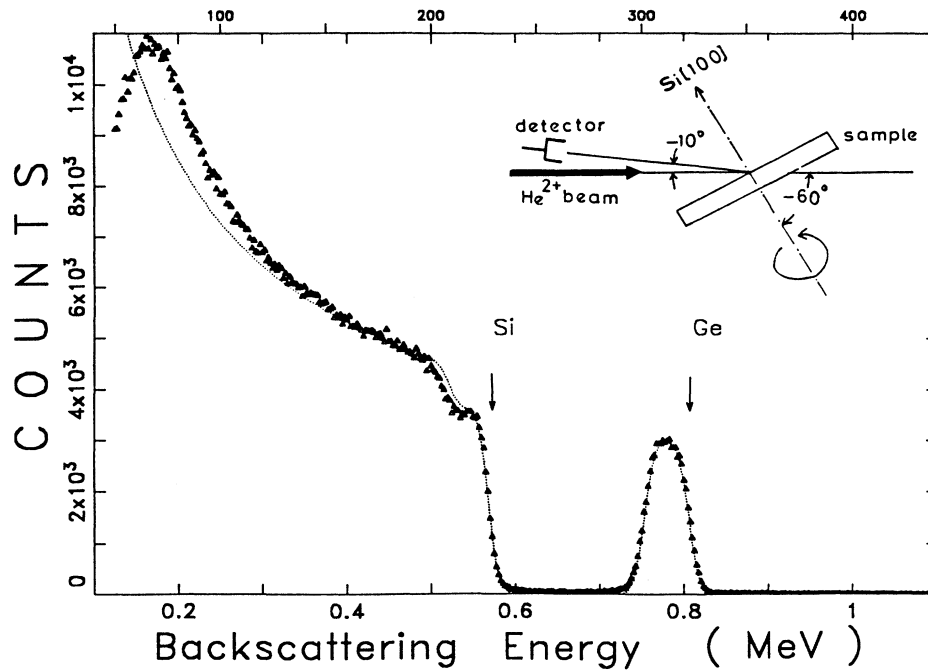


FIG. 1. RBS spectra measured (triangles) and calculated (dashed line) for MBE2 sample. Inset: sample arrangement for RBS measurements.

erford backscattering (RBS).¹⁶ Because the Ge concentration is low (6–18 at.%) and the films are thin (≤ 900 Å), high depth resolution in the RBS measurements is required to obtain accurate Ge concentrations and thicknesses. Therefore the samples were tilted by 60° with respect to the incident He ion beam, as shown in Fig. 1 (inset), and a He ion energy of 1 MeV was used. To avoid channeling effects, the samples were rotated around the axis perpendicular to the sample surface, as shown in Fig. 1 (inset). The thickness and Ge concentration for each sample were determined by fitting theoretical calculations to experimental spectra.¹⁶ As an example, the RBS result for MBE2 is shown in Fig. 1 together with the theoretical fitting. The Ge concentrations and film thicknesses thus obtained for the four films are given in Table I. Ge concentrations range from 6 to 18 at. %, thicknesses from 500 to 900 Å.

B. X-ray rocking curves

X-ray rocking curves were measured using a double crystal diffractometer with a (400) silicon monochromator and CuK_α radiation.¹⁷ The resulting XRC's for

MBE1, MBE2, CVD1, and CVD2 are shown in Fig. 2. Each rocking curve was measured for two orientations of the substrate which placed the (400) plane normal in the scattering plane and were related by rotating the sample by 180° around the scattering vector. The angular spacings $\Delta\Theta_1$ and $\Delta\Theta_2$ between the substrate (400) maximum and the (400) maximum from the Ge-containing epitaxial layer were measured for the two orientations. For each sample, the misorientation angle $\Delta\omega$ between the layer and the substrate was determined,

$$\Delta\omega = (\Delta\Theta_1 - \Delta\Theta_2) / 2, \quad (1)$$

and the value $\Delta\Theta$ corresponding to the difference in (400) plane spacing for the layer and the substrate was determined,

$$\Delta\Theta = (\Delta\Theta_1 + \Delta\Theta_2) / 2. \quad (2)$$

For each sample, the difference in (400) plane spacing for the layer and the substrate is given by

$$\left[\frac{\Delta d}{d} \right]_{\perp} = -(\cot\Theta)\Delta\Theta. \quad (3)$$

TABLE I. Ge concentrations x_{Ge} and thicknesses t obtained from RBS measurements for $\text{Si}_{1-x_{\text{Ge}}}\text{Ge}_{x_{\text{Ge}}}$ epitaxial films.

Sample	MBE1	CVD1	MBE2	CVD2
x_{Ge}	0.06 ± 0.01	0.10 ± 0.01	0.15 ± 0.02	0.18 ± 0.02
t (Å)	900 ± 50	770 ± 50	500 ± 50	620 ± 50

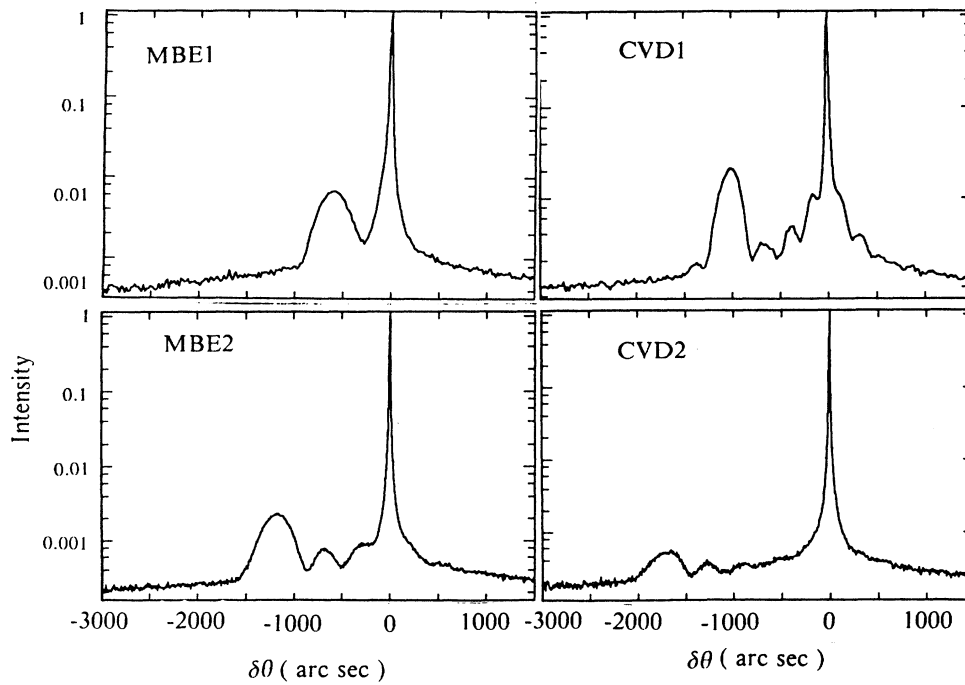


FIG. 2. Observed x-ray rocking curves for MBE1, CVD1, MBE2, and CVD2.

The misorientation angles $\Delta\omega$, differences in Bragg angles $\Delta\Theta$, and resulting values of $(\Delta d/d)_\perp$ are given in Table II for each of the samples. The misorientation angles $\Delta\omega \neq 0$ result from the small miscut of the substrates, e.g., substrate surfaces not being perfectly parallel to the (100) crystal planes.¹⁷

Because of the epitaxy between the Si-Ge films and the Si substrates, the films are expected to be tetragonal, with $(\Delta d/d)_\parallel = 0$ and with $(\Delta d/d)_\perp > (\Delta a/a)_{\text{relax}}$, where $(\Delta a/a)_{\text{relax}}$ is the fractional change in lattice parameter from added Ge for an unconstrained, cubic film. If there is complete epitaxy, e.g., no misfit dislocations at the interface of the film and substrate, $(\Delta a/a)_{\text{relax}}$ can be found from the experimentally determined value of $(\Delta d/d)_\perp$ using the relation¹⁸

$$\left(\frac{\Delta a}{a}\right)_{\text{relax}} = \frac{c_{11}}{c_{11} + 2c_{12}} \left(\frac{\Delta d}{d}\right)_\perp \quad (4)$$

with elastic constants $c_{11}/(c_{11} + 2c_{12}) = 0.564$. This is the value calculated from the elastic constants for pure Si, which we used since the difference from that for pure Ge is less than 2%,¹⁹ and theoretical calculations predict a monotonic dependence on concentration for Si-Ge alloys.²⁰ However, if there is a strain $(\Delta d/d)_\parallel \neq 0$ parallel to the substrate, i.e., partial or full incoherency between the substrate and film, Eq. (4) must be modified.¹⁸

From two XRC's for different (hkl) planes, the parallel strain $(\Delta d/d)_\parallel$ and perpendicular strain $(\Delta d/d)_\perp$ with respect to the (400) plane can be determined.²¹ We measured the XRC's of (400) and (404) planes for the MBE2 sample. The resulting value of the parallel strain was $(\Delta d/d)_\parallel = (0.1 \pm 0.4) \times 10^{-3}$, which is negligibly small compared with the perpendicular strain $(\Delta d/d)_\perp = (8.38 \pm 0.03) \times 10^{-3}$. This result confirms that the sample has very few, if any, misfit dislocations, so Eq. (4) is appropriate for calculating $(\Delta a/a)_{\text{relax}}$ from the ob-

TABLE II. Results of x-ray rocking curve measurements and lattice parameter calculations: misorientation angle $\Delta\omega$, difference in Bragg angles for film and substrate $\Delta\Theta$, fractional difference in (400) plane spacing for the film and substrate $(\Delta d/d)_\perp$, and fractional difference in relaxed lattice parameters for film and substrate obtained experimentally, $(\Delta a/a)_{\text{relax}}$, and calculated from random-solid-solution model, $(\Delta a/a)_{\text{calc}}$.

Sample	MBE1	CVD1	MBE2	CVD2
$\Delta\omega$ (deg)	0.003 ± 0.002	0.028 ± 0.002	0.007 ± 0.002	0.040 ± 0.002
$\Delta\Theta$ (deg)	-0.155 ± 0.002	-0.267 ± 0.002	-0.331 ± 0.002	-0.447 ± 0.002
$(\Delta d/d)_\perp \times 10^3$	3.93 ± 0.03	6.77 ± 0.03	8.38 ± 0.03	11.32 ± 0.03
$(\Delta a/a)_{\text{relax}} \times 10^3$	2.22 ± 0.03	3.79 ± 0.03	4.69 ± 0.03	6.34 ± 0.03
$(\Delta a/a)_{\text{calc}} \times 10^3$	1.3 ± 1.0	2.2 ± 1.5	3.5 ± 2.2	4.3 ± 2.5

served $(\Delta d/d)_1$. The present result is consistent with that of Bean *et al.*,²² which gives the critical thickness for a defect free film as 3000 Å for $x \approx 0.2$ for $\text{Si}_{1-x}\text{Ge}_x/\text{Si}(100)$ epitaxial films. Because the critical thickness increases drastically with decreasing Ge concentration,²² the other samples used in the present experiments can be treated as fully epitaxial and coherent, with negligibly few misfit dislocations.

The resultant $(\Delta a/a)_{\text{relax}}$ values are listed in Table II and are plotted in Fig. 3 vs Ge concentration. Also plotted in Fig. 3 are selected published values¹⁰ for bulk alloys. The dashed line in Fig. 3 shows Vegard's law prediction that the alloy lattice parameters vary linearly with x_{Ge} from pure Si to pure Ge. The present data for epitaxial films agree well with those of the bulk alloys, considering the uncertainties in x_{Ge} for the films, with the possible exception of sample MBE2. The dotted line and shaded area in Fig. 3 were calculated using a random-solid-solution model, as described in Sec. III.

C. Extended x-ray absorption fine structure

The Ge-Si nearest-neighbor distance $r_{\text{Ge-Si}}$ was evaluated for MBE1, MBE2, CVD1, and CVD2 samples from Ge *K*-edge EXAFS measurements. These measurements were made using the National Synchrotron Light Source beamline X23A2 with a Si (220) monochromator. Total electron yield detection²³ was used because its depth sensitivity was well matched to the present thicknesses. During the EXAFS measurements the sample was rocked around two perpendicular axes in order to avoid Bragg peak effects in the EXAFS data.²³

EXAFS results for the four samples are shown in Fig. 4. Ge *K*-edge spectra, after background subtraction and edge-jump normalization, are shown in Fig. 4(a). $\chi(k)$ functions are shown in Fig. 4(b), and radial distribution

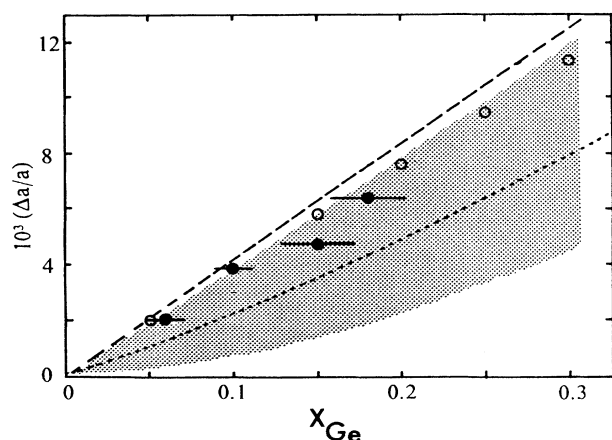


FIG. 3. $(\Delta a/a)_{\text{relax}}$ for epitaxial films (solid circles), selected values for bulk alloys (see Ref. 10) (open circles), calculated values $(\Delta a/a)_{\text{calc}}$ using the random-solid-solution model described in the text (dotted line), and the shaded area gives the range $(\Delta a/a)_{\text{calc}}$ corresponding to the $\pm 0.02\text{-}\text{\AA}$ uncertainty in $r_{\text{Ge-Si}}^{\text{NN}}$. The dashed line is Vegard's law with end-point structures pure Si and pure Ge.

functions $D_R(r)$, from transforming $k^2\chi(k)$, are shown in Fig. 4(c).

Two shells, Ge-Si and Ge-Ge, were assumed in analyzing the EXAFS data. For analyzing nearest-neighbor EXAFS, the phase shift and amplitude for Ge-Si were extracted from Ga *K*-edge EXAFS measurements on crystalline GaP, with corrections for changing the absorbing

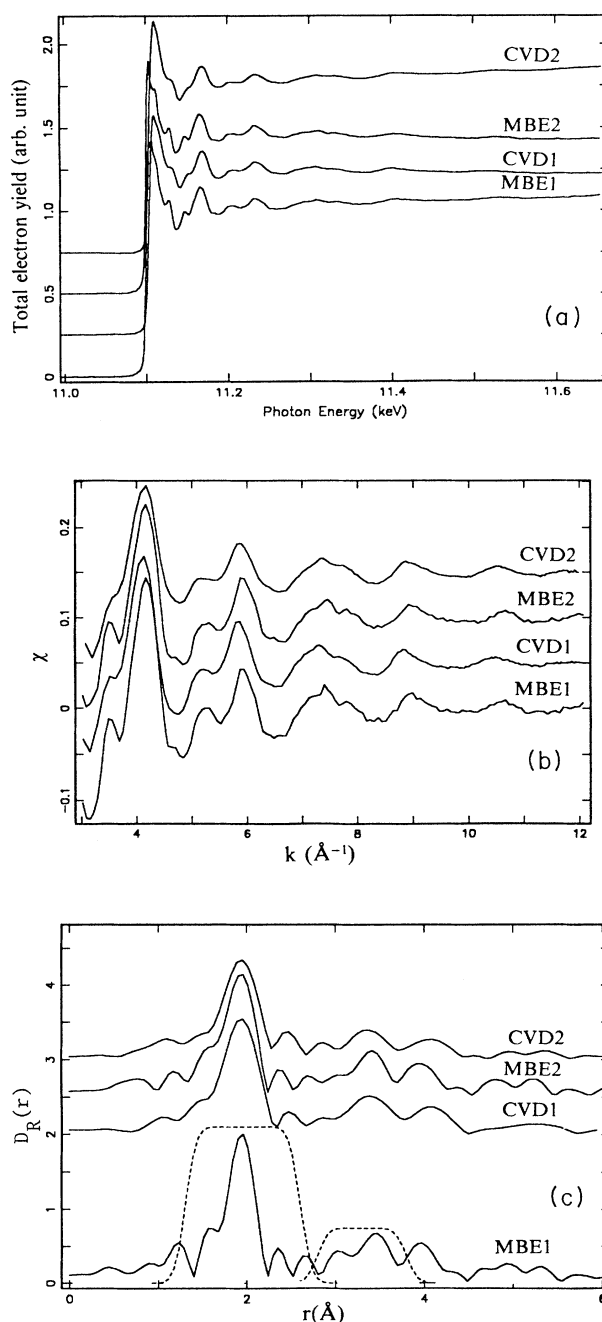


FIG. 4. EXAFS results for MBE1, CVD1, MBE2, and CVD2, (a) Ge *K*-edge spectra after background subtraction, (b) $\chi(k)$, (c) $D_R(r)$ with nearest-neighbor and next-nearest-neighbor window functions (dashed lines). Note off-set zeros for vertical axes for CVD1, MBE2, and CVD2.

atom from Ga to Ge and backscattering atom from P to Si.²⁴ The phase shift and amplitude for Ge-Ge were extracted from Ge *K*-edge EXAFS measurements on crystalline Ge. For analyzing next-nearest-neighbor EXAFS, the same phase shifts were used as for nearest neighbors. For the Ge-Si next-nearest-neighbor backscattering amplitude, the amplitude extracted for next-nearest neighbors from EXAFS measurements on a dilute ($x_{\text{As}}=0.001$) Si:As sample⁴ was used. For Ge-Ge next-nearest neighbors, the amplitude extracted for next-nearest neighbors from EXAFS measurements on crystalline Ge was used.

Quantitative information on local structure around Ge atoms was obtained by fitting calculated model functions $\chi_{\text{cal}}(k)$ for $k=3.8-12.0 \text{ \AA}^{-1}$ to the corresponding experimental functions $\chi_{\text{NN}}(k)$ and $\chi_{\text{NNN}}(k)$ obtained by back-transforming nearest-neighbor and next-nearest-neighbor regions of $D_R(r)$ using the window functions shown in Fig. 4(c).⁴ The total coordination number $N_{\text{Ge-Si}} + N_{\text{Ge-Ge}}$ was fixed at 4 for nearest neighbors and at 12 for next-nearest neighbors. The contribution from Ge-Ge pairs was too small to permit accurate determinations of the Ge-Ge distance even for the $x_{\text{Ge}}=0.18$ sample. For definiteness and to aid in sample-to-sample comparisons $r_{\text{Ge-Ge}}$ was fixed at 2.45 \AA , in nearest-neighbor fitting for all samples. For next-nearest-neighbor fitting, it was assumed that $r_{\text{Ge-Si}}^{\text{NNN}} = r_{\text{Ge-Ge}}^{\text{NNN}}$.

Standard deviations were calculated for each of the structural parameters determined by linearized least-square fitting. These error estimates shown in Table III correspond to the range of values which increase the mean-square fitting error $\sum[\chi_{\text{NN}}(k_i) - \chi_{\text{calc}}(k_i)]^2$ for $k=3.8-12.0 \text{ \AA}^{-1}$ by no more than 100%, and similarly for next-nearest neighbors.⁴ The fitted $\chi_{\text{NN}}(k)$ and $\chi_{\text{NNN}}(k)$ functions for MBE1 sample are shown in Figs. 5(a) and 5(b). The deduced interatomic distances for nearest neighbors $r_{\text{Ge-Si}}^{\text{NN}}$ and for next-nearest neighbors r^{NNN} are shown in Fig. 6 and are given together with nearest-neighbor and next-nearest-neighbor coordination numbers in Table III. Within experimental uncertainties, Ge-to-Si nearest-neighbor distances, $r_{\text{Ge-Si}}^{\text{NN}} = (2.37 \sim 2.38 \pm 0.02) \text{ \AA}$, do not vary much with composition and are $0.02 \sim 0.03 \text{ \AA}$ larger than the usual Si-to-Si nearest-neighbor distance in pure crystalline Si, in agree-

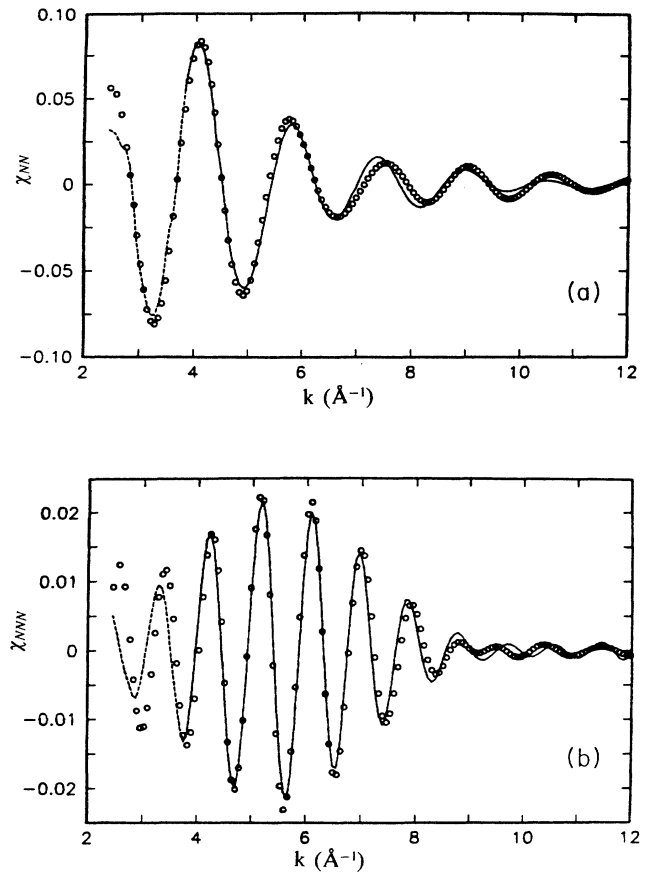


FIG. 5. Fitting for (a) nearest neighbors with back-transformed $\chi_{\text{NN}}(k)$ and (b) next-nearest-neighbors $\chi_{\text{NNN}}(k)$. Open circles indicate experiments; line, model calculations.

ment with the result recently reported by Woicik *et al.*¹² for a Si-Ge alloy film with $x_{\text{Ge}}=0.31$, and with the previous results by Incoccia *et al.*¹³ for amorphous Si-Ge alloys. Next-nearest-neighbor distances for the alloys do not vary with composition and they are unchanged from those of pure Si, within experimental uncertainties. The nearest-neighbor and next-nearest-neighbor coordination

TABLE III. Results of EXAFS measurements: Ge-to-Si nearest-neighbor distance $r_{\text{Ge-Si}}^{\text{NN}}$; Ge-Ge and Ge-Si nearest-neighbor coordination numbers $N_{\text{Ge-Si}}^{\text{NN}}$ and $N_{\text{Ge-Ge}}^{\text{NN}}$, next-nearest-neighbor distances r^{NNN} , next-nearest-neighbor coordination numbers $N_{\text{Ge-Si}}^{\text{NNN}}$ and $N_{\text{Ge-Ge}}^{\text{NNN}}$, and correction to Ge-Si nearest-neighbor distance calculated for coherency strain Δr_{corr} .

Sample	MBE1	CVD1	MBE2	CVD2
$r_{\text{Ge-Si}}^{\text{NN}}$	2.37 ± 0.02	2.38 ± 0.02	2.37 ± 0.02	2.38 ± 0.02
$N_{\text{Ge-Si}}^{\text{NN}}$	3.7 ± 0.5	3.7 ± 0.5	3.7 ± 0.5	3.3 ± 0.6
$N_{\text{Ge-Ge}}^{\text{NN}}$	0.3 ± 0.5	0.3 ± 0.5	0.3 ± 0.5	0.7 ± 0.6
r^{NNN}	3.85 ± 0.06	3.85 ± 0.06	3.85 ± 0.06	3.84 ± 0.06
$N_{\text{Ge-Si}}^{\text{NNN}}$	11.5 ± 2	11.5 ± 4	11 ± 2	9 ± 3
$N_{\text{Ge-Ge}}^{\text{NNN}}$	0.5 ± 2	0.5 ± 4	1 ± 2	3 ± 3
Δr_{corr}	0.002	0.004	0.005	0.006

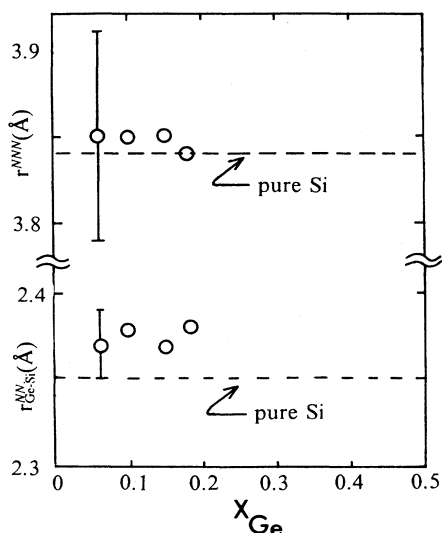


FIG. 6. Near-neighbor distances r^{NN} and r^{NNN} vs Ge concentration x_{Ge} . The dashed lines are the nearest-neighbor and next-nearest-neighbor distances for pure crystalline Si.

numbers are consistent, within their large uncertainties, with Si and Ge forming a random solid solution, e.g., $N_{\text{Ge-Ge}}^{\text{NN}}/4 = N_{\text{Ge-Ge}}^{\text{NNN}}/12 = x_{\text{Ge}}$.

III. DISCUSSION

First we discuss the correction of local interatomic distances obtained from EXAFS measurements on the epitaxial films required because the films are constrained by their substrates. This lattice constraint causes macroscopic elastic strains parallel ϵ_{\parallel} and perpendicular ϵ_{\perp} to the substrate, as well as corresponding local atomic bond-length strains $\Delta r/r$ and local atomic bond-angle strains $\Delta\theta/\theta$. When a film has a diamond cubic structure and a (100) coherent growth plane with its substrate, $\Delta r/r$ can be deduced from ϵ_{\parallel} and ϵ_{\perp} if the strain is assumed to be homogeneous, with the same bond-length changes $\Delta r/r$ for Ge—Si, Si—Si, and Ge—Ge bonds, and with no bond-angle changes. Neglect of bond angle changes permits the following estimate of Δr_{corr} , an upper bound on the actual value,

$$\frac{\Delta r_{\text{corr}}}{r} = 1 - \left[1 + \frac{4}{3}\epsilon_{\parallel} \left[1 - \frac{c_{12}}{c_{11}} \right] \right]^{1/2}, \quad (5)$$

where $\Delta r_{\text{corr}} = r - r'$, and r and r' are relaxed and constrained nearest-neighbor distances, respectively. c_{11} and c_{12} are elastic constants. The corrections Δr_{corr} for Ge-Si nearest-neighbor distances were calculated using elastic constants for Si and values of $\epsilon_{\parallel} = -(\Delta a/a)_{\text{relax}}$ from Table II, and they are given in Table III. The largest correction is indicated for CVD2, $\Delta r_{\text{corr}} = +0.006 \text{ \AA}$, which is nevertheless smaller than other uncertainties in our nearest-neighbor distances, 0.02 \AA . If full coherency is maintained for films with larger Ge concentrations, this type of correction will be larger for the larger Ge

concentrations. For $x_{\text{Ge}} = 0.3$, this approach yields $\Delta r_{\text{corr}} = +0.012 \text{ \AA}$. Woicik *et al.*² have taken a different approach in examining effects of coherency strain on local structure by considering both bond-angle distortions and bond-length distortions. For the case of an epitaxial film with $x_{\text{Ge}} = 0.3$, they conclude that $\Delta r_{\text{corr}} = 0.007 \text{ \AA}$ and that the bond angles are reduced by $\Delta\theta = 1.4^\circ$. As expected, their value of $\Delta r_{\text{corr}}/r$ is smaller than our upper bound calculation.

Now we discuss the relationship between nearest-neighbor bond lengths and lattice parameters for substitutional alloys. For a random solid solution with an average lattice which is diamond cubic, as for $\text{Si}_{1-x}\text{Ge}_x$, the lattice parameter a , which is measured by x-ray diffraction, is related to the average nearest-neighbor bond length $\langle r \rangle = (\sqrt{3}/4)a$, and

$$\begin{aligned} \langle r \rangle = & x_{\text{Ge}}^2 \bar{r}_{\text{Ge-Ge}} + (1 - x_{\text{Ge}})^2 \bar{r}_{\text{Si-Si}} \\ & + 2x_{\text{Ge}}(1 - x_{\text{Ge}}) \bar{r}_{\text{Ge-Si}}, \end{aligned} \quad (6)$$

where $\bar{r}_{\text{Ge-Ge}}$ is the average Ge-Ge nearest-neighbor bond length for the random solid solution of composition x_{Ge} and can be measured, for example, by EXAFS.²⁵

In general, the average bond lengths $\bar{r}_{\text{Ge-Ge}}$, $\bar{r}_{\text{Si-Si}}$, and $\bar{r}_{\text{Ge-Si}}$ are expected to be composition dependent, so that $\bar{r}_{\text{Ge-Ge}} = \bar{r}_{\text{Ge-Ge}}(x_{\text{Ge}})$, etc. Composition dependence of bond lengths in such systems has been discussed by Martins and Zunger,⁷ Shih *et al.*,⁸ and Thorpe and Garboczi⁹ in terms of “natural” bond lengths and bond-bending and bond-stretching force constants β and α . It is beyond the scope of the present paper to compare and contrast the various approaches to this question. In general the composition dependence of a bond length depends upon β and α . If $\beta \gg \alpha$ for an alloy AB , bond lengths adjust to minimize bond-angle distortions and $\langle r \rangle = \bar{r}_{AB} = \bar{r}_{AA} = \bar{r}_{BB}$. If $\alpha \gg \beta$, the bond angles adjust to accommodate the various differing bond lengths, $r_{AB} = \bar{r}_{AB} = r_{AB}^0$, where r_{AB}^0 is the natural bond length.

In the present case $r_{\text{Ge-Si}}^{\text{NN}} = \bar{r}_{\text{Ge-Si}}$ is measured directly²⁵ to be $2.375 \pm 0.02 \text{ \AA}$, and we observe negligible dependence $\pm 0.02 \text{ \AA}$ of this bond length on composition for $x_{\text{Ge}} = 0.06 - 0.18$. In this range we assume that $\bar{r}_{\text{Si-Si}}$ changes negligibly and is given by $\bar{r}_{\text{Si-Si}}^0 = 2.35 \text{ \AA}$, and that $\bar{r}_{\text{Ge-Ge}}$, which occurs quite infrequently, is given by $\bar{r}_{\text{Ge-Ge}}^0 = 2.45 \text{ \AA}$.

We then proceed to calculate $\langle r(x_{\text{Ge}}) \rangle$ and $a(x_{\text{Ge}})$ using Eq. (6). The resulting values of

$$\left[\frac{\Delta a}{a} \right]_{\text{calc}} = \frac{a(x_{\text{Ge}}) - a_{\text{Si}}}{a_{\text{Si}}} \quad (7)$$

are given in Table II and are shown in Fig. 3 as a dotted line. The major uncertainty in the calculated values (see shaded region of Fig. 3) comes from the $\pm 0.02 \text{ \AA}$ uncertainty in the EXAFS results for $r_{\text{Ge-Si}}$. Within these uncertainties, the calculated values of $a(x_{\text{Ge}})$ are consistent with the measured values, although much better agreement would be obtained with $\bar{r}_{\text{Ge-Si}} = 2.395 \text{ \AA}$.

Another approach for relating nearest-neighbor bond lengths and overall lattice parameters makes more expli-

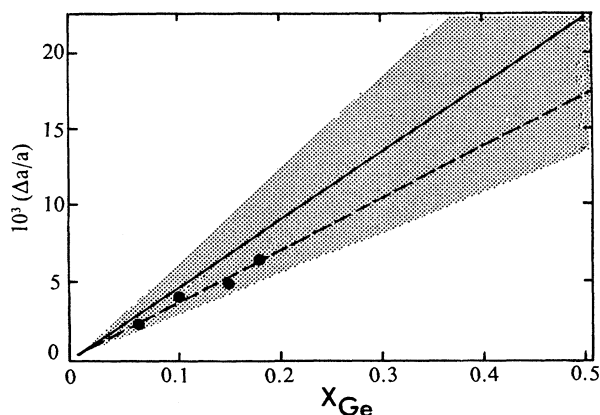


FIG. 7. Vegard's law with end-point structures pure Si ($r_{\text{Si-Si}}^0 = 2.35 \text{ \AA}$) and hypothetical zinc-blende SiGe compound with $r_{\text{Ge-Si}}^0 = 2.404 \pm 0.02 \text{ \AA}$ (solid line) or $2.392 \pm 0.02 \text{ \AA}$ (dashed line) as discussed in the text. The shaded region gives the range of $(\Delta a/a)$ for $\pm 0.02 \text{ \AA}$ uncertainty in $r_{\text{Ge-Si}}^0$ for the former case (2.404 \AA). The latter case has a similar range of uncertainty. Also repeated here are the actual values of $(\Delta a/a)_{\text{relax}}$ from Fig. 3.

cit use of Vegard's law, as follows. For the case of $\text{Ge}_{x_{\text{Ge}}}\text{Si}_{1-x_{\text{Ge}}}$ with $x_{\text{Ge}} < 0.5$, there are two plausible ways to apply Vegard's law. The most straightforward way is to take pure Si and pure Ge as the end-point phases. This method involves only Si—Si and Ge—Ge bond lengths and predicts lattice parameters for Ge—Si alloys which are somewhat larger than those observed experimentally (see the dashed line in Fig. 3). Another approach, which involves only Si—Si and Ge—Si bond lengths, is to take pure Si and a hypothetical zinc-blende SiGe compound as the end-point phases. If the Ge—Si bond length in the SiGe compound is smaller than the average bond lengths for Si—Si and Ge—Ge in the pure elements, then Vegard's law based on Si and Si—Ge will predict lattice parameters for Si—Ge alloys which are smaller than the predictions from using pure Si and Ge for the end-point phases.

Predicting the Ge—Si bond length for the SiGe compound, presumed to be the natural Ge—Si bond length $r_{\text{Ge-Si}}^0$, requires extrapolation from the values of $r_{\text{Ge-Si}}$ determined from EXAFS measurements for $0.06 \leq x_{\text{Ge}} \leq 0.18$. Both Martins and Zunger⁷ and Shih *et al.*⁸ give prescriptions for calculating the natural bond length from bond-length measurements made in the dilute limit $r_{\text{Ge-Si}}(0)$,

$$\frac{r_{\text{Ge-Si}}(0) - r_{\text{Si-Si}}^0}{r_{\text{Ge-Si}}^0 - r_{\text{Si-Si}}^0} = \epsilon, \quad (8)$$

where Martins and Zunger⁷ calculate ϵ from bond-stretching and bond-bending force constants for Si and Ge, $\epsilon = 0.58$, and Shih *et al.*⁸ obtain $\epsilon = 0.75$ by neglecting both bond-bending force constants and movements of second shell neighbors.²⁶ Thorpe and Garboczi⁹ argue that the approach of Shih *et al.*⁸ is fundamentally flawed

and gives approximately the right answer only because of cancellation of errors in ignoring both bond-bending forces and movements of second shell neighbors.

Using $\epsilon = 0.58$ and the EXAFS results for $r_{\text{Ge-Si}}(0)$ gives $r_{\text{Ge-Si}}^0 = 2.404 \pm 0.02 \text{ \AA}$, and using $\epsilon = 0.75$ gives $2.392 \pm 0.02 \text{ \AA}$. Vegard's-law predictions for $a(x_{\text{Ge}})$ with these two values for the natural Ge—Si bond length are shown in Fig. 7 as $(\Delta a/a)_{\text{calc}}$. Within the experimental uncertainties of the EXAFS results, both agree with the observed composition dependence of lattice parameters for Ge—Si alloys. However, this approach is expected to predict lattice parameters which are somewhat too small. Even for $x_{\text{Ge}} < 0.5$ there are expected to be some Ge—Ge nearest-neighbor bonds as well as Si—Si and Ge—Si bonds, since the alloys are actually disordered solid solutions. Including the longer Ge—Ge bonds, as was done in the random-solid-solution model discussed earlier, would increase the average bond lengths and therefore the lattice parameter with respect to those calculated with this form of Vegard's law.

IV. CONCLUSIONS

Observed values for $r_{\text{Ge-Si}}(x_{\text{Ge}})$ with $x_{\text{Ge}} = 0.06-0.18$ were $2.375 \pm 0.02 \text{ \AA}$ only $0.02-0.03 \text{ \AA}$ larger than the usual Si—Si nearest-neighbor distance in pure Si, 2.35 \AA . For next-nearest neighbors surrounding Ge atoms, the observed distance, $3.85 \pm 0.05 \text{ \AA}$, was the same as for pure Si, 3.84 \AA , within the experimental accuracy.

Effects of coherency strain on observed nearest-neighbor distances were estimated to be less than 0.006-\AA compression for $x_{\text{Ge}} = 0.18$ and to be even smaller for the more dilute samples, in all cases smaller than our experimental uncertainties.

Lattice parameters for the epitaxial Ge—Si films, obtained from x-ray rocking curves and corrected for coherency strains, agreed well with lattice parameters previously reported for bulk Ge—Si alloys. The composition dependence of lattice parameters for Ge—Si alloys was well reproduced by a simple random-solid-solution model using an average nearest-neighbor distance calculated from the Ge—Si nearest-neighbor distances determined from EXAFS measurements and the Si—Si and Ge—Ge distances taken from the pure elements.

Another approach to predicting the alloy lattice parameters using Vegard's law and the natural Ge—Si bond length, taking into account bond-bending and bond-stretching force constants and the EXAFS result for the Ge—Si bond length in Si-rich alloys, also gave satisfactory results.

The present work, for an isovalent substitutional impurity, Ge in Si, verifies that EXAFS measurements can be used to predict the effect of the impurity on lattice parameter using procedures similar to those employed to determine the "size effect" contribution to lattice parameter changes for heterovalent substitutional impurities, As and Ga in Si, in earlier studies.^{2,3,5}

ACKNOWLEDGMENTS

We thank R. Thompson and B. S. Meyerson for providing MBE and CVD samples, respectively; A Marwick

and G. Coleman for assistance with measurements and analysis of RBS, J. Angilello and R. F. Boehme for assistance with XRC and EXAFS measurements, L. W. Hobbs and M. F. Thorpe for helpful discussions, and J. C. Woicik for providing us before publication a copy of his work¹² on bond lengths and lattice parameters in

strained GeSi layers. This research was carried out in part at the National Synchrotron Light Source, Brookhaven National Laboratory, which is supported by the U.S. Department of Energy, Division of Materials Sciences and Division of Chemical Sciences (DOE Contract No. DE-AC02-76CH00016).

*Permanent address: Miyagi National College of Technology, Natori, Miyagi 981-12, Japan.

[†]Present address: Laboratoire pour l'Utilisation du Rayonnement Electromagnétique, Centre Universitaire de Paris-Sud, 91405 Orsay CEDEX, France.

¹L. Vegard, *Z. Phys.* **5**, 17 (1921).

²G. S. Cargill III, J. Angilello, and K. L. Kavanaugh, *Phys. Rev. Lett.* **61**, 1748 (1988); see also, J. M. Tonnerre, M. Matsuura, G. S. Cargill III, and L. W. Hobbs, in *Defects in Materials*, edited by P. D. Bristowe, J. E. Epperson, J. E. Griffith, and Z. Lilienthal-Weber, MRS Symposia Proceedings No. 209 (Materials Research Society, Pittsburgh, 1991), p. 505.

³A. Parisini, A. Bourret, A. Armigliato, M. Servidori, S. Solmi, R. Fabbri, J. R. Regnard, and J. L. Allain, *J. Appl. Phys.* **67**, 2320 (1990).

⁴A. Erbil, W. Weber, G. S. Cargill, and R. F. Boehme, *Phys. Rev. B* **34**, 1392 (1986).

⁵K. L. Kavanagh, G. S. Cargill III, R. F. Boehme, and J. C. P. Chang, in *Ion Beam Processing of Advanced Electronic Materials*, edited by N. Cheung, J. Roberto, and A. Marwick, MRS Symposia Proceedings No. 147 (Materials Research Society, Pittsburgh, 1989), p. 53; K. L. Kavanagh, J. C. P. Chang, and G. S. Cargill III (unpublished).

⁶Preliminary results were reported by M. Matsuura, J. M. Tonnerre, and G. S. Cargill III, *Bull. Am. Phys. Soc.* **35**, 281 (1990).

⁷J. L. Martins and A. Zunger, *Phys. Rev. B* **30**, 6217 (1984).

⁸C. K. Shih, W. E. Spicer, W. A. Harrison, and A. Sher, *Phys. Rev. B* **31**, 1139 (1985).

⁹M. F. Thorpe and E. J. Garboczi, *Bull. Am. Phys. Soc.* **35**, 781 (1990); unpublished.

¹⁰See J. P. Dismukes, L. Ekstrom and R. J. Paff, *J. Phys. Chem.* **68**, 3021 (1964), and earlier references listed therein.

¹¹K. Takeda, A. Taguchi, and M. Sakata, *J. Phys. C* **16**, 2237 (1983).

¹²J. C. Woicik, C. E. Bouldin, M. I. Bell, J. O. Cross, D. J. Tweet, B. D. Swanson, T. M. Zhand, L. B. Sorensen, C. A.

King, J. L. Hoyt, P. Pianetta, and J. F. Gibbons, *Phys. Rev. B* **43**, 2419 (1991).

¹³L. Incoccia, S. Mobilio, M. G. Proietti, P. Florini, C. Giovannella, and F. Evangelisti, *Phys. Rev. B* **31**, 1028 (1985).

¹⁴R. D. Thompson, S. S. Iyer, and S. L. Delage, *Electrochem. Soc. Proc.* **88-8**, 582 (1988).

¹⁵B. S. Meyerson, K. J. Uram, and F. K. LeGoues, *Appl. Phys. Lett.* **53**, 2555 (1988).

¹⁶See, for example, W. Chu, J. W. Mayer and M. Nicolet, *Backscattering Spectroscopy* (Academic, New York, 1978).

¹⁷See, for example, C. R. Wie, T. A. Tombrello and T. Vreeland, Jr., *J. Appl. Phys.* **59**, 3743 (1989); V. S. Speriosu, *ibid.* **52**, 6094 (1981).

¹⁸J. Hornstra and W. J. Bartels, *J. Crystal Growth* **44**, 513 (1978).

¹⁹H. J. McSkimin and P. Andreatch Jr., *J. Appl. Phys.* **35**, 2161 (1964); **34**, 651 (1963).

²⁰T. Soma, Y. Katabira, and H. Matsuo, *Phys. Status Solidi B* **110**, K167 (1982).

²¹K. Ishida, J. Matsui, T. Kamejima, and I. Sakuma, *Phys. Status Solidi A* **31**, 255 (1975).

²²J. C. Bean, L. C. Feldman, A. T. Fiory, S. Nakahara, and I. K. Robinson, *J. Vac. Sci. Technol. A* **2**, 436 (1984).

²³A. Erbil, G. S. Cargill III, R. Frahm, and R. F. Boehme, *Phys. Rev. B* **37**, 2450 (1988).

²⁴P. A. Lee, P. H. Citrin, P. Eisenberger, and B. M. Kincaid, *Rev. Mod. Phys.* **53**, 769 (1981).

²⁵The values of $r_{\text{Ge-Si}}$ determined from EXAFS measurements for each alloy represent averages for Ge atoms in different near-neighbor environments in that disordered alloy. Although the averaging inherent in the EXAFS measurement and analysis may not be exact [see P. Eisenberger and G. S. Brown, *Solid State Commun.* **29**, 481 (1979)], we nevertheless use the EXAFS result $r_{\text{Ge-Si}}^{\text{NN}}$ for $\bar{r}_{\text{Ge-Si}}$.

²⁶ ϵ in Eq. (8), without subscripts, is used to keep the notation of Ref. 7. Its meaning is unrelated to those of the symbols ϵ_{\parallel} and ϵ_{\perp} used earlier in this section.